Chapter 4

An ε- uniform convergent scheme for the singularly perturbed parabolic partial differential equations with an interior turning point

4.1 Introduction

There are some articles in the literature (see Chapter 1), in which the methods for the solution of singularly perturbed turning point problems (SPTPPs) in the context of ODEs were considered. To the best of our knowledge, the development of the numerical schemes for the solution of SPTPBVPs for PDEs is at initial stage.

In this chapter, a parameter-uniform scheme is proposed for singularly perturbed parabolic partial differential equations with an interior turning point whose solution exhibit twin boundary layers. To resolve the boundary, a fitted-mesh is constructed and the cubic B-spline basis functions on this mesh are used to discretize the given equation. Asymptotic bounds are given for the analytic solution and its derivatives. Through a brief analysis, the method is shown uniformly convergent irrespective of the parameter ε with first-order accuracy in t and the second-order accuracy (up to a logarithm factor) in x. Two test problems are encountered to validate the theoretical results.

Let $\Omega = (-1,1)$, $\Lambda = (0,T]$, $D = \Omega \times \Lambda$, $\Gamma_b = \{(x,0) : -1 \le x \le 1\}$, $\Gamma_l = \{(-1,t) : 0 \le t \le T\}$, $\Gamma_r = \{(1,t) : 0 \le t \le T\}$ and $\Gamma = \Gamma_l \cup \Gamma_b \cup \Gamma_r$. We consider the following SPTPBVP on the rectangular domain D

$$L_\varepsilon y(x,t) \equiv -y_t(x,t) + \varepsilon y_{xx}(x,t) + a(x,t)y_x(x,t) - b(x,t)y(x,t) = f(x,t), \quad (x,t) \in D, \tag{4.1a}$$

$$y(x,0) = y_0(x), \quad x \in \Omega, \tag{4.1b}$$

$$y(-1,t) = \phi_l(t), \quad \text{on} \quad \Gamma_l, \tag{4.1c}$$

$$y(1,t) = \phi_r(t), \quad \text{on} \quad \Gamma_r, \tag{4.1d}$$

where ε is a small parameter. The point $x \in (-1,1)$ at which $a(x,t)$ vanishes is called a turning point and the problem (4.1) is called a turning point problem. In this chapter, we consider the case in which there is a unique x at which the coefficient of convective term vanishes and it changes sign in the neighborhood of x. The location of the boundary layer(s) or interior layer(s) depends upon the behavior of the functions $a(x,t)$ and $b(x,t)$ near the turning point. All the functions involved in the problem (4.1) are assumed to be bounded and sufficiently smooth. Furthermore, we consider the following assumptions

$$A1: \ a(0,t) = 0, \quad a_x(0,t) < 0, \ 0 \le t \le T. \tag{4.2a}$$

$$A2: \ |a(x,t)| \ge \alpha > 0, \quad 0 < \gamma \le |x| \le 1, \ 0 \le t \le T \tag{4.2b}$$

$$A3: \ b(x,t) \ge \beta > 0, \quad (x,t) \in D. \tag{4.2c}$$

$$A4: \ |a_x(x,t)| \ge \frac{|a_x(0,t)|}{2}, \quad (x,t) \in D. \tag{4.2d}$$

Assumptions A1 and A2 ensure the existence of twin boundary layers in the solution of (4.1). The assumption A3 ensures that the operator L_ε in (4.1a) satisfies the maximum principle and the so called resonance phenomena [41] is excluded. Finally, assumption A4 guarantees the uniqueness of the turning point. Furthermore, under the assumptions (4.2), the SPTPBVP (4.1) has a unique solution exhibiting twin boundary layers.

The remainder of the chapter is organized as follows. In Section 4.2, some *a priori* estimates are given associated with the continuous problem (4.1). In Section 4.3, the temporal semi-discretization on a uniform mesh by means of the Euler implicit scheme is given and the global error estimate is obtained. In the same section, the B spline functions on a piecewise-uniform mesh are used to discretize the system of ODEs obtained in the temporal semi-discretization. The proposed method is shown as parameter-uniform convergent in Section 4.4 followed by the numerical experiments and the discussions on the results in Section 4.5. Finally, in the last section 4.6, some

concluding remarks are drawn.

4.2 Some Analytical Results: A Priori Estimates

First, we show that the operator L_ε satisfies the following lemma.

Lemma 4.2.1 (Minimum Principle)**.** *Let $\Phi \in C^{2,1}(\bar{D})$ be non-negative on Γ and $L_\varepsilon\Phi$ is non-positive in D. Then, Φ is non-negative throughout $\bar{D}$.*

Proof. Our aim is to prove that Φ is non-negative in D. For contrary assume that the minimum of $\Phi(x,t)$ is negative that occurs at $(\theta,\zeta) \in D$. Then, it is easy to verify that $L_\varepsilon\Phi(\theta,\zeta) > 0$ and thus we obtain the result. □

Lemma 4.2.2 (Stability Estimate)**.** *The solution $y(x,t)$ of (4.1) satisfies the following parameter-uniform bound on $\bar{D}$*

$$\|y\|_{\bar{D}} \leq \|y\|_\Gamma + \frac{\|f\|_{\bar{D}}}{\beta}.$$

Proof. The barrier functions $\Pi^\pm(x,t) = \|y\|_\Gamma + \frac{\|f\|_{\bar{D}}}{\beta} \pm y(x,t)$ satisfy

$$\begin{aligned}
\Pi^\pm(-1,t) &= \|y\|_\Gamma + \frac{\|f\|_{\bar{D}}}{\beta} \pm y(-1,t) \geq \|y\|_\Gamma \pm y(-1,t) \geq 0,\\
\Pi^\pm(1,t) &= \|y\|_\Gamma + \frac{\|f\|_{\bar{D}}}{\beta} \pm y(1,t) \geq \|y\|_\Gamma \pm y(1,t) \geq 0,\\
\Pi^\pm(x,0) &= \|y\|_\Gamma + \frac{\|f\|_{\bar{D}}}{\beta} \pm y(x,0) \geq \|y\|_\Gamma \pm y(x,0) \geq 0.
\end{aligned}$$

Also, at all (x,t) in D

$$L_\varepsilon\Pi^\pm(x,t) = -b\left[\|y\|_\Gamma + \frac{\|f\|_{\bar{D}}}{\beta}\right] \pm L_\varepsilon y(x,t) \leq -\beta\|y\|_\Gamma - \|f\|_{\bar{D}} \pm f \leq -\|f\|_{\bar{D}} \pm f \leq 0.$$

The proof is completed by using the minimum principle. □

We split the interval $\bar{\Omega}$ as $\bar{\Omega} = \Omega_1 \cup \Omega_2 \cup \Omega_3$, where $\Omega_1 = [-1,-\gamma]$, $\Omega_2 = [-\gamma,\gamma]$ and $\Omega_3 = [\gamma,1]$ and $0 < \gamma \leq 1/2$. The following theorem gives the bounds on the mixed derivatives of the solution of (4.1) in the intervals which exclude the turning point.

Theorem 4.2.1. *Suppose $a(x,t)$, $b(x,t)$, and $f(x,t)$ are $C^{2+r,1+r/2}(\bar{D})$, $0<r<1$ functions and the compatibility conditions are satisfied. Then for $0\le l\le 3$, $0\le l+m\le 3$, we have*

$$\left|\frac{\partial^{l+m}y}{\partial x^l\partial t^m}\right|\le\begin{cases}C\left(1+\dfrac{e^{-\frac{\xi(1+x)}{\varepsilon}}}{\varepsilon^l}\right), & x\in\Omega_1,\\ C\left(1+\dfrac{e^{-\frac{\xi(1-x)}{\varepsilon}}}{\varepsilon^l}\right), & x\in\Omega_3.\end{cases}$$

Here ξ and C are generic positive constants.

The following theorem shows that the mixed derivatives of the solution of problem (4.1) near the turning point $x=0$ (since $b(0,t)/a_x(0,t)<0$) are bounded.

Theorem 4.2.2. *Under the assumptions of Theorem 4.2.1, we have*

$$\left|\frac{\partial^{l+m}y}{\partial x^l\partial t^m}\right|\le C,\quad x\in\Omega_2.$$

4.3 Numerical Scheme: The Discretization

4.3.1 Semi-discretization for time variable

In this section, the Euler implicit rule is used for time semi-discretization on the domain defined as:

$$\Lambda^M=\{t_k=k\delta t:\ k=0,1,\ldots,M,\ t_0=0,\ t_M=T\},$$

Then the problem (4.1) on $\Omega\times\Lambda^M$ is discretized as:

$$-D_t^-Y^{k+1}(x)+\varepsilon(Y_{xx})^{k+1}+a^{k+1}(x)(Y_x)^{k+1}-b^{k+1}(x)Y^{k+1}=f^{k+1}(x),\ 0\le k\le M-1,$$

$$Y^{k+1}(-1)=\phi_l(t_{k+1}),\quad Y^{k+1}(1)=\phi_r(t_{k+1}),\quad 0\le k\le M-1,$$

$$Y^{k+1}(x)=y_0(x),\quad x\in\Omega,$$

where $Y^{k+1}(x)$ is the approximation of $Y(x,t_{k+1})$. Now using $D_t^- v_i^k = \frac{v_i^k - v_i^{k-1}}{\delta t}$, we obtain

$$\begin{cases} \hat{L}_\varepsilon Y^{k+1}(x) = g^{k+1}(x), & x \in \Omega,\ 0 \le k \le M-1, \\ Y^{k+1}(-1) = \phi_l(t_{k+1}), \quad Y^{k+1}(1) = \phi_r(t_{k+1}), & 0 \le k \le M-1, \\ Y^{k+1}(x) = y_0(x), & x \in \Omega, \end{cases} \tag{4.3}$$

where

$$g^{k+1}(x) = f^{k+1}(x) - \frac{Y^k(x)}{\delta t}, \quad d^{k+1}(x) = -b^{k+1}(x) - \frac{1}{\delta t},$$

and the operator $\hat{L}_\varepsilon$ is defined as

$$\hat{L}_\varepsilon Y^{k+1}(x) \equiv \varepsilon (Y_{xx})^{k+1}(x) + a^{k+1}(x)(Y_x)^{k+1}(x) + d^{k+1}(x) Y^{k+1}(x).$$

Lemma 4.3.1 (Minimum Principle)**.** *Suppose that* $\varphi^{k+1}(-1) \ge 0,\ \varphi^{k+1}(1) \ge 0$ *and* $\hat{L}_\varepsilon \varphi^{k+1}(x) \le 0, \forall\, x \in \Omega$ *then* $\varphi^{k+1}(x) \ge 0, \forall\, x \in \bar{\Omega}$.

Proof. For contrary assume $\varphi^{k+1}(s) = \min_{x\in\Omega} \varphi^{k+1}(x) < 0$. It can easily follows that $\hat{L}_\varepsilon \varphi^{k+1}(s) > 0$, and thus the result is obtained. □

The bound on the local truncation error e_{k+1} is given by the following lemma.

Lemma 4.3.2. *The local error estimate in the temporal direction is given by*

$$\|e_{k+1}\| \le C(\delta t)^2.$$

Proof. For the proof, see [124]. □

The bound on the global error E_k which is the measure of the contribution of the local error estimate at each time step is given by the following lemma.

Lemma 4.3.3. *The global error estimate at* t_k *is given by*

$$\|E_k\| \le C\delta t, \quad k \le T/\delta t.$$

Proof. We have

$$\begin{aligned}\|E_k\| &= \left\| \sum_{i=1}^{k} e_i \right\|, \quad k \leq \frac{T}{\delta t} \\ &\leq \|e_1\| + \|e_2\| + \cdots + \|e_k\| \\ &\leq Ck(\delta t)^2 \\ &= C(\delta t).\end{aligned}$$

□

The following theorem estimates the bounds on the solution $Y^{k+1}(x)$ of (4.3) and its derivatives.

Theorem 4.3.1. *For $l = 0,1,2,3$ the solution $Y^{k+1}(x)$ of (4.3) and its derivatives satisfy the following estimates*

$$\left| \frac{d^l Y^{k+1}(x)}{dx^l} \right| \leq \begin{cases} C\left(1 + \dfrac{e^{-\frac{\xi(1+x)}{\varepsilon}}}{\varepsilon^l}\right), & x \in \Omega_1, \\ C, & x \in \Omega_2, \\ C\left(1 + \dfrac{e^{-\frac{\xi(1-x)}{\varepsilon}}}{\varepsilon^l}\right), & x \in \Omega_3, \end{cases}$$

where C and ξ are generic positive constants.

4.3.2 The spatial discretization

The system of ODEs (4.3) obtained in the previous section is further discretized to obtain the fully discretized scheme on a piecewise-uniform mesh generated as follows: Divide the interval $[-1,1]$ into three non-overlapping subintervals $[-1,-1+\kappa]$, $(-1+\kappa, 1-\kappa]$, and $(1-\kappa,1]$, where κ is given by

$$\kappa = \min\left\{\frac{1}{4}, \kappa_0 \varepsilon \ln N\right\},$$

where $\kappa_0 \geq \frac{1}{\alpha}$ is a constant and $N = 2^m$ ($m \geq 3$). Then a fitted piecewise-uniform mesh $\bar{\Omega}^N = \{x_l\}_{l=0}^N$ is generated as

$$x_l = \begin{cases} -1 + lh_l, & \text{if} \quad l = 0, 1, \ldots, \frac{N}{4}, \\ (-1+\kappa) + \left(l - \frac{N}{4}\right) h_l, & \text{if} \quad l = \frac{N}{4}+1, \ldots, \frac{3N}{4}, \\ (1-\kappa) + \left(l - \frac{3N}{4}\right) h_l, & \text{if} \quad l = \frac{3N}{4}+1, \ldots, N, \end{cases}$$

with the mesh spacing

$$h_l = \begin{cases} \frac{4\kappa}{N}, & \text{if} \quad l = 1, 2, \ldots, \frac{N}{4}, \\ \frac{4(1-\kappa)}{N}, & \text{if} \quad l = \frac{N}{4}+1, \ldots, \frac{3N}{4}, \\ \frac{4\kappa}{N} & \text{if} \quad l = \frac{3N}{4}+1, \ldots, N. \end{cases}$$

Clearly, the mesh is uniform when $\kappa = 1/4$ otherwise it is dense in the boundary layer region and coarse otherwise. The fitted piecewise-uniform mesh $D^{N,M}$ on D is then defined as the tensor product $D^{N,M} = \Omega^N \times \Lambda^M$. In the proof of the ε-uniform convergence, we need the following lemma.

Lemma 4.3.4. *For a fixed mesh and for all positive integers k, we have*

$$\lim_{\varepsilon \to 0} \max_{1 \leq l \leq N-1} \frac{e^{-\frac{\xi(1+x_l)}{\varepsilon}}}{\varepsilon^k} \to 0.$$

Proof. For the proof the readers are referred to [125]. □

The interval $[-1, 1]$ is divided into the elements $[x_l, x_{l+1}]$, $l = 0, \ldots, N-1$ with piecewise-uniform spacing defined in the previous section. The cubic B-splines R_l, $l = -1, 0, \ldots, N+1$ at the nodes x_l are defined to form a basis over the interval $[-1, 1]$

(see Ref. [126]) as follows

$$R_l(x)=\frac{1}{h_l^3}\begin{cases}(x-x_{l-2})^3, & [x_{l-2},x_{l-1}],\\ h_l^3+3h_l^2(x-x_{l-1})+3h_l(x-x_{l-1})^2-3(x-x_{l-1})^3, & [x_{l-1},x_l],\\ h_l^3+3h_l^2(x_{l+1}-x)+3h_l(x_{l+1}-x)^2-3(x_{l+1}-x)^3, & [x_l,x_{l+1}],\\ (x_{l+2}-x)^3, & [x_{l+1},x_{l+2}],\\ 0, & \text{otherwise.}\end{cases} \tag{4.4}$$

For simplicity we write $\hat{y}(x)$ for $Y^{k+1}(x)$ (the solution at $(k+1)$-th time level). We seek an approximation $S(x)$ to $\hat{y}(x)$ expressed as

$$S(x)=\sum_{l=-1}^{N+1}\beta_l R_l(x), \tag{4.5}$$

where β_l are the parameters to be determined by the discretized form of the equation and the boundary conditions. Two extra cubic splines R_{-1} and R_{N+1} are introduced to satisfy the boundary conditions. The values of $R_l(x)$, $R_l'(x)$ and $R_l''(x)$ at the knots calculated from (4.4) are given in the following Table.

x	x_{l-1}	x_l	x_{l+1}	otherwise
$R_l(x)$	1	4	1	0
$R_l'(x)$	$-\frac{3}{h_l}$	0	$\frac{3}{h_l}$	0
$R_l''(x)$	$\frac{6}{h_l^2}$	$-\frac{12}{h_l^2}$	$\frac{6}{h_l^2}$	0

Using the approximation $S(x)$ at the nodal points in (4.3), we get

$$q_l^-\beta_{l-1}+q_l^c\beta_l+q_l^+\beta_{l+1}=\tilde{g}_l,\quad 0\le l\le N, \tag{4.6a}$$

where

$$\begin{aligned} q_l^- &= \frac{6\varepsilon}{h_l^2}-\frac{3}{h_l}\tilde{a}_l+\tilde{d}_l,\\ q_l^c &= \frac{-12\varepsilon}{h_l^2}+4\tilde{d}_l,\\ q_l^+ &= \frac{6\varepsilon}{h_l^2}+\frac{3}{h_l}\tilde{a}_l+\tilde{d}_l, \end{aligned}$$

and $\tilde{a}_l = a^{k+1}(x_l)$, $\tilde{d}_l = d^{k+1}(x_l)$, $\tilde{g}_l = g^{k+1}(x_l)$. The given boundary conditions become

$$\beta_{-1} + 4\beta_0 + \beta_1 = \phi_l(t_{k+1}), \tag{4.6b}$$

$$\beta_{N-1} + 4\beta_N + \beta_{N+1} = \phi_r(t_{k+1}). \tag{4.6c}$$

Thus on eliminating β_{-1} and β_{N+1} from (4.6a)-(4.6c), we obtain the following $(N+1)\times(N+1)$ linear system

$$AX = F,$$

where A is the tri-diagonal matrix given by

$$A = \begin{pmatrix} -4q_0^- + q_0^c & -q_0^- + q_0^+ & 0 & \dots & \dots & \dots & \dots & 0 \\ A_1(x_1) & A_2(x_1) & A_3(x_1) & 0 & 0 & \dots & \dots & 0 \\ 0 & A_1(x_2) & A_2(x_2) & A_3(x_2) & 0 & \dots & \dots & 0 \\ \vdots & \ddots & \ddots & \ddots & \vdots & \vdots & \vdots & \vdots \\ \dots & \dots & \dots & \dots & 0 & A_1(x_{N-1}) & A_2(x_{N-1}) & A_3(x_{N-1}) \\ 0 & \dots & \dots & \dots & \dots & 0 & q_N^- - q_N^+ & q_N^c - 4q_N^+ \end{pmatrix}.$$

The elements of A are given by

$$\begin{aligned} A_1(x_l) &= q_l^-, \quad 1 \le l \le N-1, \\ A_2(x_l) &= q_l^c, \quad 1 \le l \le N-1, \\ A_3(x_l) &= q_l^+, \quad 1 \le l \le N-1. \end{aligned}$$

The column vectors X and F are given as

$$X = \begin{pmatrix} \beta_0 \\ \beta_1 \\ \vdots \\ \beta_N \end{pmatrix}, \quad F = \begin{pmatrix} \tilde{g}_0 - \phi_l(t_{k+1})q_0^- \\ \tilde{g}_1 \\ \tilde{g}_2 \\ \vdots \\ \tilde{g}_N - \phi_r(t_{k+1})q_N^+ \end{pmatrix}.$$

4.4 Parameter Uniform Convergence Analysis

In this section, we will prove that the proposed method converges quadratically (up to a logarithmic factor) and independent of ε in the spatial direction. The following lemma which shows that the sum of absolute values of all spline functions are bounded will be used in error analysis.

Lemma 4.4.1. *The set $\{R_l(x)\}_{l=-1}^{N+1}$ of B-splines satisfies*

$$\sum_{l=-1}^{N+1} |R_l(x)| \leq 10, \quad x \in \bar{\Omega}.$$

Proof. Using the definition of cubic B-splines the proof is easy. □

Theorem 4.4.1. *Let $S(x)$ be the approximation to $\hat{y}(x)$ and $\tilde{g} \in C^2(\bar{\Omega})$. Then*

$$\sup_{0<\varepsilon\leq 1} \max_{0\leq l\leq N} |\hat{y}(x_l) - S(x_l)| \leq CN^{-2}(\ln N)^3.$$

Proof. We estimate the error in $[-1,0]$, similar estimates can be obtained in $[0,1]$ by using the similar approach. The unique spline interpolate $U_N(x)$ to the solution of (4.3) is given by

$$U_N(x) = \sum_{l=-1}^{N+1} \bar{\beta}_l R_l(x).$$

If $\tilde{g}(x) \in C^2(\bar{\Omega})$ then $\hat{y}(x) \in C^4(\bar{\Omega})$ and so the estimates given in [127] yields

$$\|(\hat{y} - U_N)^{(j)}\| \leq \lambda_j \|\hat{y}^{(4)}\| \bar{h}^{4-j}, \quad j = 0,1,2, \tag{4.7}$$

where λ_j are the constants. It helps us to estimate

$$\begin{aligned}
|\hat{L}_\varepsilon \hat{y}(x_l) - \hat{L}_\varepsilon U_N(x_l)| &\leq \varepsilon |\hat{y}''(x_l) - U_N''(x_l)| + |a(x_l)||\hat{y}'(x_l) - U_N'(x_l)| \\
&\quad + |d(x_l)||\hat{y}(x_l) - U_N(x_l)| \\
&\leq (\varepsilon\lambda_2 \bar{h}^2 + \|a\|\lambda_1 \bar{h}^3 + \|d\|\lambda_0 \bar{h}^4))|\hat{y}^{(4)}(x_l)| \\
&\leq C\left(\varepsilon\lambda_2 \bar{h}^2 + \|a\|\lambda_1 \bar{h}^3 + \|d\|\lambda_0 \bar{h}^4 \left(1 + \frac{e^{-\frac{\xi(1+x_l)}{\varepsilon}}}{\varepsilon^4}\right)\right).
\end{aligned} \tag{4.8}$$

Now depending on the magnitude of κ there arises the following two cases. In the first case $\kappa = 1/4$, it is easy to get

$$|\hat{L}_\varepsilon \hat{y}(x_l) - \hat{L}_\varepsilon U_N(x_l)| \leq CN^{-2}(\ln N)^3, \quad 1 \leq l \leq N/2. \tag{4.9}$$

On the other hand in the second case $\kappa = \kappa_0 \varepsilon \ln N$, we have $h_l = \frac{4\kappa}{N}$ for $1 \leq l \leq N/4$ and $h_l = \frac{4(1-\kappa)}{N}$ for $N/4+1 \leq l \leq N/2$. For $N/4+1 \leq l \leq N/2$ *i.e.,* in the regular region, using (4.3.1), we have immediately from (4.8)

$$|\hat{L}_\varepsilon \hat{y}(x_l) - \hat{L}_\varepsilon U_N(x_l)| \leq CN^{-2}. \tag{4.10}$$

Also, for $1 \leq l \leq \frac{N}{4}$, $\bar{h} = 4\tau/N = 4\kappa_0 \varepsilon N^{-1} \ln N$, and so $\bar{h}/\varepsilon = CN^{-1} \ln N$. Then using Lemma 4.3.4, we obtain

$$|\hat{L}_\varepsilon \hat{y}(x_l) - \hat{L}_\varepsilon U_N(x_l)| \leq CN^{-2}(\ln N)^2. \tag{4.11}$$

The inequality (4.10) together with (4.11) yields

$$|\hat{L}_\varepsilon \hat{y}(x_l) - \hat{L}_\varepsilon U_N(x_l)| \leq CN^{-2}(\ln N)^2, \, 1 \leq l \leq \frac{N}{2}. \tag{4.12}$$

Therefore, on combining both cases, we obtain

$$|\hat{L}_\varepsilon S(x_l) - \hat{L}_\varepsilon U_N(x_l)| = |\tilde{g}(x_l) - \hat{L}_\varepsilon U_N(x_l)| \tag{4.13}$$

$$= |\hat{L}_\varepsilon \hat{y}(x_l) - \hat{L}_\varepsilon U_N(x_l)| \leq CN^{-2}(\ln N)^3, \; 1 \leq l \leq N/2. \tag{4.14}$$

Now considering the linear system $A\bar{X} = \bar{F}$ associated with $\hat{L}_\varepsilon U_N(x_l) = \bar{g}(x_l)$, $U_N(x_0) = \phi_l(t_{k+1})$, $U_N(x_N) = \phi_r(t_{k+1})$ yields

$$A(X - \bar{X}) = F - \bar{F}, \tag{4.15}$$

where

$$X - \bar{X} = \begin{pmatrix} \beta_0 - \bar{\beta}_0 \\ \beta_1 - \bar{\beta}_1 \\ \vdots \\ \beta_N - \bar{\beta}_N \end{pmatrix}, \qquad F - \bar{F} = \begin{pmatrix} \tilde{g}(x_0) - \bar{g}(x_0) \\ \tilde{g}(x_1) - \bar{g}(x_1) \\ \vdots \\ \tilde{g}(x_N) - \bar{g}(x_N) \end{pmatrix}.$$

Thus using (4.13), we obtain

$$\|F - \bar{F}\| \leq CN^{-2}(\ln N)^3. \tag{4.16}$$

It can be seen that for small h_l, except the first and last row of A

$$|a_{l,l}| - (|a_{l,l-1}| + |a_{l,l+1}|) = -6d_l > 0.$$

Also, for the first and last row of A, we have

$$|a_{0,0}| - |a_{0,1}| = \frac{36\varepsilon}{h_0^2} - \frac{18a_0}{h_0},$$

and

$$|a_{N,N}| - |a_{N,N-1}| = \frac{36\varepsilon}{h_N^2} + \frac{6a_N}{h_N}.$$

Therefore, from the estimate given in [128]

$$\|A^{-1}\| \leq C,$$

and thus (4.15) and (4.16) yield

$$\|X - \bar{X}\| \leq CN^{-2}(\ln N)^3. \tag{4.17}$$

Now it is easy to see from the boundary conditions (4.6b)-(4.6c)

$$|\beta_{-1} - \bar{\beta}_{-1}| \leq CN^{-2}(\ln N)^3, \tag{4.18}$$

and

$$|\beta_{N+1} - \bar{\beta}_{N+1}| \leq CN^{-2}(\ln N)^3. \tag{4.19}$$

Equations (4.17)-(4.19) together give

$$\max_{-1 \leq l \leq N+1} |\beta_l - \bar{\beta}_l| \leq CN^{-2}(\ln N)^3.$$

Thus, we are enable to estimate $|S(x)-U_N(x)|$ as

$$|S(x)-U_N(x)| \leq \max_{-1\leq l\leq N+1} |\beta_l-\bar{\beta}_l| \sum_{l=-1}^{N+1} |R_l(x)| \leq CN^{-2}(\ln N)^3,$$

and so,

$$\max_{0\leq l\leq N} |S(x_l)-U_N(x_l)| \leq CN^{-2}(\ln N)^3.$$

Finally, the use of the triangle inequality yields

$$\sup_{0<\varepsilon\leq 1} \max_{0\leq l\leq N} |\hat{y}(x_l)-S(x_l)| \leq CN^{-2}(\ln N)^3. \qquad \square$$

The following parameter-uniform convergence theorem is the consequence of the Lemma 4.3.3 and Theorem 4.4.1

Theorem 4.4.2. *Let $S(x_l)$ be the approximation to the solution $\hat{y}(x_l)$ of the problem (4.1) at $(k+1)$-th time level of the fully discretized scheme after the temporal discretization. Then,*

$$|S(x_l)-\hat{y}(x_l)| \leq C(\delta t + N^{-2}(\ln N)^3), \quad 0\leq l\leq N.$$

4.5 Numerical Illustrations

Example 4.5.1. Consider the following test problem

$$\begin{aligned} -y_t+\varepsilon y_{xx}-(t+1)xy_x-(4+t)y &= e^{-t}x(1-x), \quad (x,t)\in D,\\ y(x,0)=1,\ x\in\bar{\Omega}, &\quad y(-1,t)=y(1,t)=1,\ t\in\bar{\Lambda}=[0,1]. \end{aligned}$$

Example 4.5.2. Consider the following test problem

$$\begin{aligned} -y_t+\varepsilon y_{xx}-x(t^2+1)y_x-(2+t)y &= 10t^2e^{-t}x(1-x), \quad (x,t)\in D,\\ y(x,0)=1+x^2,\ x\in\bar{\Omega}, &\quad y(-1,t)=y(1,t)=2,\ t\in\bar{\Lambda}=[0,1]. \end{aligned}$$

Since the analytical/exact solutions are unavailable so for a fixed ε, we compute

$$e_{\varepsilon}^{N,M} = \max_{k} \left(\max_{l} |S^{2N,2M}(x_{2l}, t_{2k}) - S^{N,M}(x_l, t_k)| \right),$$

a variant of double mesh principle, to observe the accuracy (maximum absolute error) of the proposed scheme. Here $S^{N,M}(x_l, t_k)$ and $S^{2N,2M}(x_{2l}, t_{2k})$ are the numerical solutions obtained on $D^{N,M}$ and $D^{2N,2M}$ respectively. The mesh $D^{N,M}$ is used to obtain $D^{2N,2M}$ by using the interpolation. The computed order of convergence is estimated as

$$p_{\varepsilon}^{N,M} = \frac{\log(e_{\varepsilon}^{N,M}) - \log(e_{\varepsilon}^{2N,2M})}{\log 2}.$$

The ε-uniform pointwise error $p^{N,M}$ is estimated by taking the maximum of $e_{\varepsilon}^{N,M}$ over $\varepsilon = 1, 2^{-4}, 2^{-8}, \ldots, 2^{-32}$ *i.e.,*

$$e^{N,M} = \max_{\varepsilon = 1, 2^{-4}, 2^{-8}, \ldots, 2^{-32}} e_{\varepsilon}^{N,M}.$$

We also compute the parameter-uniform order of convergence $p^{N,M}$ as

$$p^{N,M} = \frac{\log(e^{N,M}) - \log(e^{2N,2M})}{\log 2}.$$

Table 4.1: $e_\varepsilon^{N,M}, e^{N,M}, p_\varepsilon^{N,M}$ and $p^{N,M}$ for Example 4.5.1.

	N					
ε	32	64	128	256	512	1024
2^0	1.55e-02	8.03e-03	4.09e-03	2.06e-03	1.04e-03	5.19e-04
	0.95	0.97	0.99	0.99	1.00	
2^{-4}	2.86e-02	5.95e-03	2.95e-03	1.49e-03	7.48e-04	3.75e-04
	2.26	1.01	0.99	0.99	1.00	
2^{-8}	4.74e-01	1.21e-01	4.12e-02	1.13e-02	3.50e-03	1.07e-03
	1.97	1.55	1.87	1.69	1.71	
2^{-12}	2.74e-01	1.20e-01	4.10e-02	1.12e-02	3.50e-03	1.07e-03
	1.19	1.55	1.87	1.68	1.71	
2^{-16}	2.70e-01	1.19e-01	4.09e-02	1.12e-02	3.50e-03	1.07e-03
	1.18	1.54	1.87	1.68	1.71	
2^{-20}	2.84e-01	1.19e-01	4.09e-02	1.12e-02	3.50e-03	1.07e-03
	1.25	1.54	1.87	1.68	1.71	
$\vdots$	$\vdots$	$\vdots$	$\vdots$	$\vdots$	$\vdots$	
2^{-32}	2.85e-01	1.19e-01	4.09e-02	1.12e-02	3.51e-03	1.07e-03
	1.26	1.54	1.87	1.67	1.71	
$e^{N,M}$	4.74e-01	1.21e-01	4.12e-02	1.13e-02	3.50e-03	1.07e-03
$p^{N,M}$	1.97	1.55	1.87	1.69	1.71	

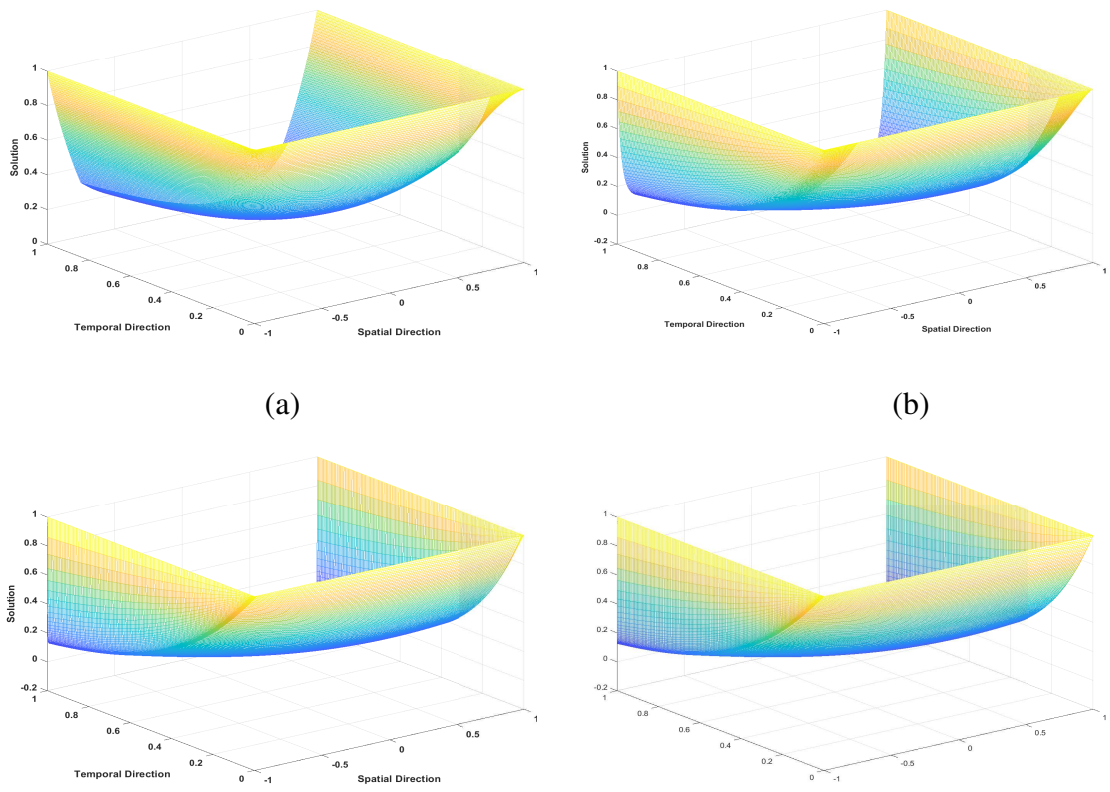

Figure 4.1: Numerical solution profiles for Example 4.5.1 (a) $\varepsilon = 1$ (b) $\varepsilon = 2^{-4}$ (c) $\varepsilon = 2^{-8}$ and (d) $\varepsilon = 2^{-12}$.

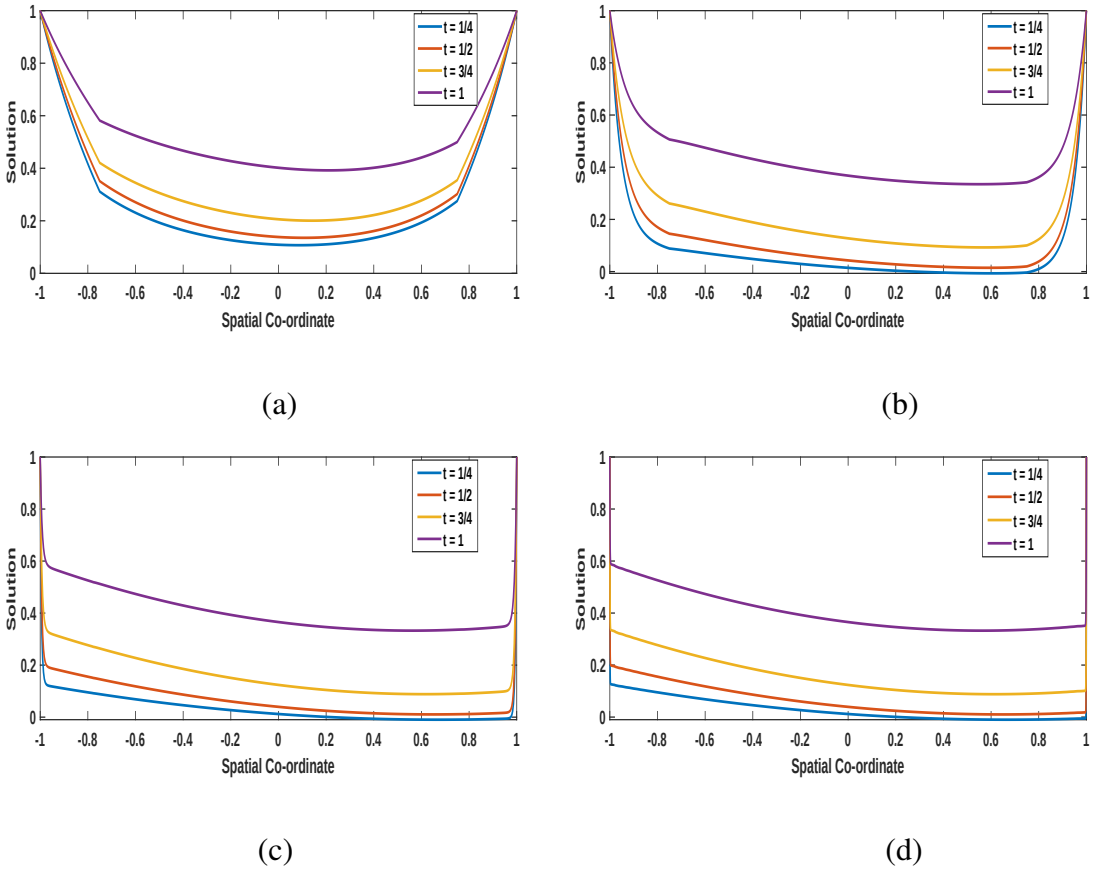

Figure 4.2: Numerical solution profiles for Example 4.5.1 for different time levels (a) $\varepsilon = 1$ (b) $\varepsilon = 0.1$ (c) $\varepsilon = 0.01$ and (d) $\varepsilon = 0.001$.

Table 4.2: $e_\varepsilon^{N,M}, e^{N,M}, p_\varepsilon^{N,M}$ and $p^{N,M}$ for Example 4.5.2.

	N					
ε	32	64	128	256	512	1024
2^0	2.44e-02	1.23e-02	6.84e-03	4.21e-03	2.69e-03	1.77e-03
	0.99	0.85	0.70	0.65	0.60	
2^{-4}	5.49e-02	1.63e-02	8.21e-03	4.12e-03	2.06e-03	1.03e-03
	1.75	0.99	0.99	1.00	1.00	
2^{-8}	9.55e-01	2.46e-01	8.40e-02	2.31e-02	7.23e-03	2.22e-03
	1.97	1.55	1.86	1.67	1.70	
2^{-12}	5.42e-01	2.46e-01	8.44e-02	2.33e-02	7.43e-03	2.69e-03
	1.14	1.54	1.86	1.65	1.47	
2^{-16}	5.61e-01	2.46e-01	8.45e-02	2.33e-02	7.44e-03	2.95e-03
	1.19	1.54	1.86	1.65	1.33	
2^{-20}	5.90e-01	2.46e-01	8.45e-02	2.33e-02	7.44e-03	2.97e-03
	1.26	1.54	1.86	1.65	1.32	
$\vdots$	$\vdots$	$\vdots$	$\vdots$	$\vdots$	$\vdots$	
2^{-32}	5.92e-01	2.46e-01	8.45e-02	2.33e-02	7.44e-03	2.97e-03
	1.27	1.54	1.86	1.65	1.32	
$e^{N,M}$	9.55e-01	2.46e-01	8.45e-02	2.33e-02	7.44e-03	2.97e-03
$p^{N,M}$	1.96	1.54	1.86	1.65	1.32	

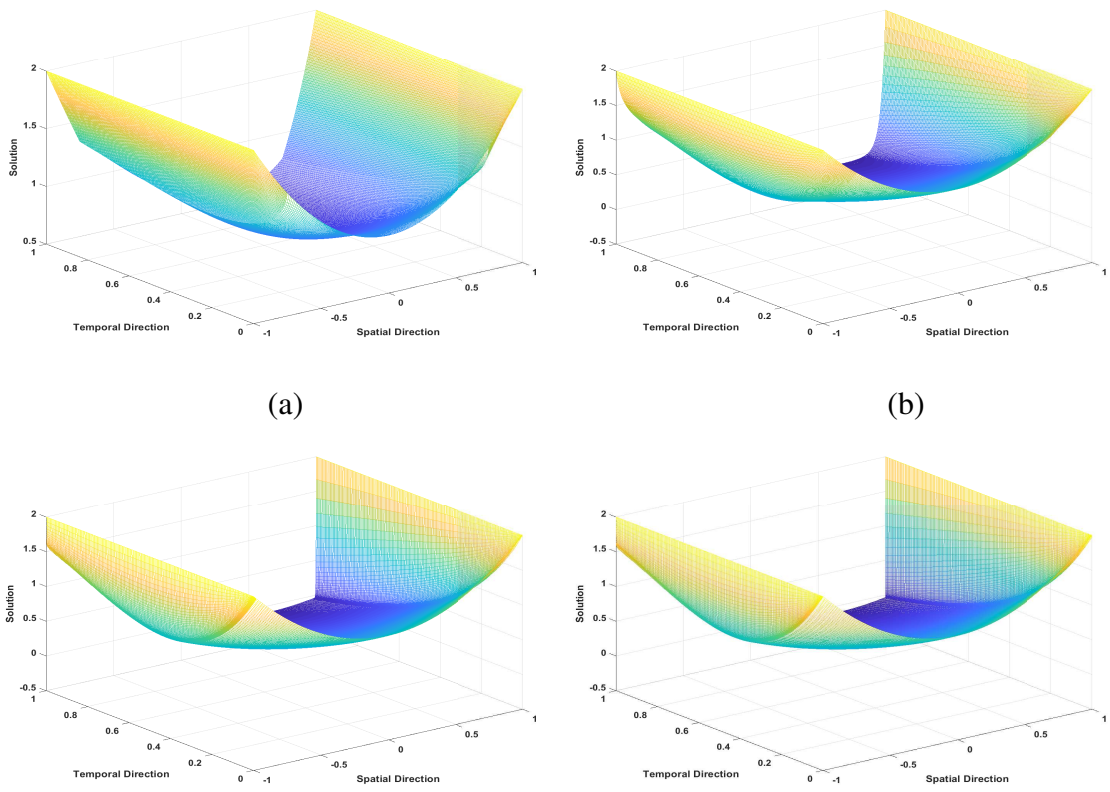

Figure 4.3: Numerical solution profiles for Example 4.5.2 (a) $\varepsilon = 1$ (b) $\varepsilon = 2^{-4}$ (c) $\varepsilon = 2^{-8}$ and (d) $\varepsilon = 2^{-12}$.

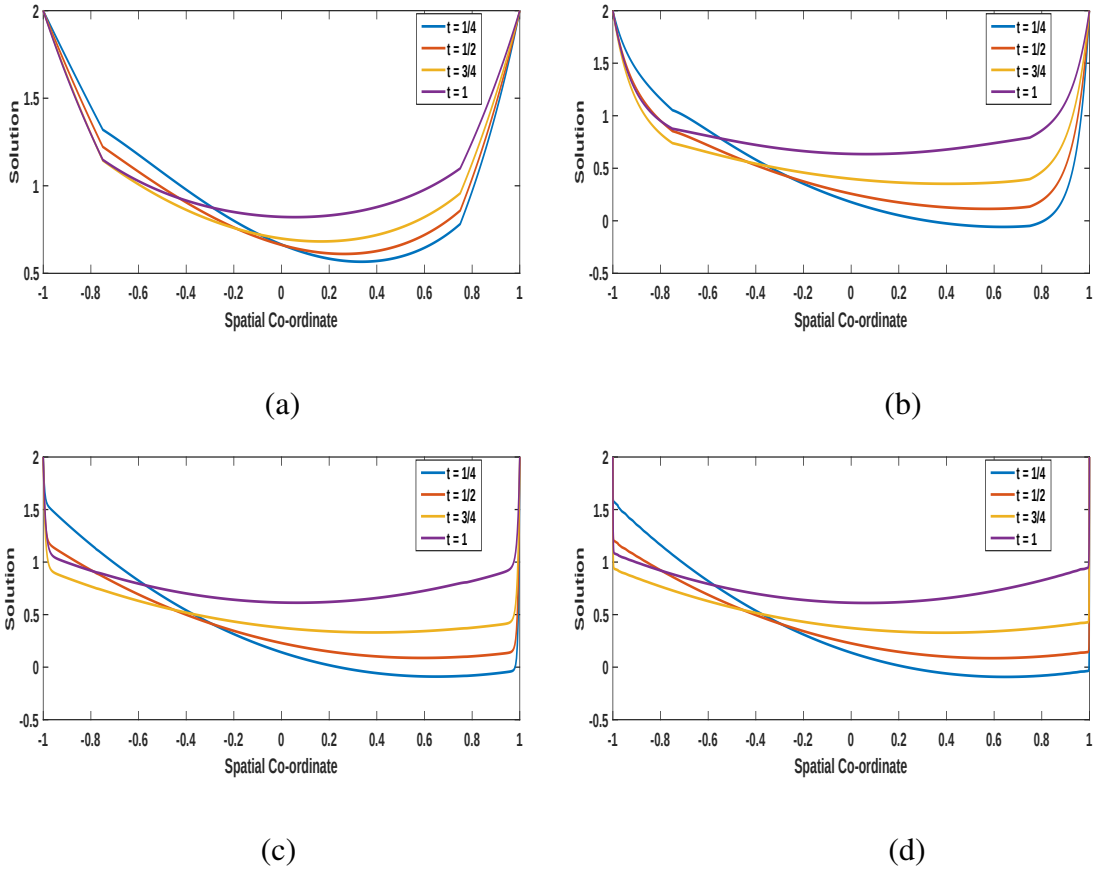

Figure 4.4: Numerical solution profiles for Example 4.5.2 for different time levels (a) $\varepsilon = 1$ (b) $\varepsilon = 0.1$ (c) $\varepsilon = 0.01$ and (d) $\varepsilon = 0.001$.

The numerical results presented in the Tables 4.1 and 4.2 clearly indicate that the convergence is independent of ε and is in a very good agreement with the bounds given in Theorem 4.4.2. All the results presented in Tables 4.1 and 4.2 are obtained by taking $\kappa_0 = 4$ and $\delta t = 1/N$. Also, all the graphs have been plotted by taking $\delta t = 1/N = 2^{-8}$. To observe the change in the boundary layer width with respect to the parameter and to show the physical phenomenon of the solution, the surface plots (refer Figs. 4.1 and 4.3) have been presented. These figures clearly indicate that the solution of the test problems exhibit twin boundary layers at $x = -1$ and $x = 1$ for small ε close to zero, and the boundary layer width decreases as the parameter decreases. To see the solution at some individual time steps, the solution behavior for different time levels are plotted in Figs. 4.2 and 4.4 respectively.

4.6 Conclusion

Due to the presence of the boundary/interior layers in their solutions the SPTPBVPs especially for PDEs are difficult to solve using standard/classical methods. Usually, when seeking for the numerical solutions of such problems (layer problems), layer adapted meshes *i.e.,* the meshes which are fine in the layer region and coarse otherwise should be used. These meshes, especially when time is involved, make the computation more complex with regards to the convergence analysis. In this chapter, we have designed and analysed a collocation method on a fitted-mesh for the solution of a class of time dependent SPTPBVPs whose solution exhibits twin boundary layers. We established sharp bounds (without proof) on the solution and its derivatives which were used to prove the ε-uniform convergence of the proposed scheme. Two test problems are encountered to confirm the order of ε-uniform convergence numerically which is proved theoretically in Theorem 4.4.2.